



1

2 **A bulk-mass-modeling-based method for retrieving Particulate Matter Pollution using**
3 **CALIOP observations**

4

5

6 Travis D. Toth¹, Jianglong Zhang², Jeffrey S. Reid³, and Mark A. Vaughan¹

7

8 ¹NASA Langley Research Center, Hampton, VA

9 ²Department of Atmospheric Sciences, University of North Dakota, Grand Forks, ND

10 ³Marine Meteorology Division, Naval Research Laboratory, Monterey, CA

11

12

13 *Correspondence to:* Travis D. Toth (travis.d.toth@nasa.gov); Jianglong Zhang

14 (jianglong.zhang@und.edu)

15

16

17 **Abstract.** In this proof-of-concept paper, we apply a bulk-mass-modeling method using
18 observations from the NASA Cloud-Aerosol Lidar with Orthogonal Polarization (CALIOP)
19 instrument for retrieving particulate matter (PM) concentration over the contiguous United States
20 (CONUS) over a 2-year period (2008-2009). Different from previous approaches that rely on
21 empirical relationships between aerosol optical depth (AOD) and PM_{2.5} (PM with particle sizes
22 less than 2.5 μm), for the first time, we derive PM_{2.5} concentrations, both at daytime and nighttime,
23 from near surface CALIOP aerosol extinction retrievals using bulk mass extinction coefficients
24 and model-based hygroscopicity. Preliminary results from this 2-year study conducted over the
25 CONUS show a good agreement ($r^2 \sim 0.48$; mean bias of $-3.3 \mu\text{g m}^{-3}$) between the averaged
26 nighttime CALIOP-derived PM_{2.5} and ground-based PM_{2.5} (with a lower r^2 of ~ 0.21 for daytime;
27 mean bias of $-0.4 \mu\text{g m}^{-3}$), suggesting that PM concentrations can be obtained from active-based
28 spaceborne observations with reasonable accuracy. Results from sensitivity studies suggest that
29 accurate aerosol typing is needed for applying CALIOP measurements for PM_{2.5} studies. Lastly,
30 the e-folding correlation length for surface PM_{2.5} is found to be around 600 km for the entire
31 CONUS (~ 300 km for Western CONUS and ~ 700 km for Eastern CONUS), indicating that



32 CALIOP observations, although sparse in spatial coverage, may still be applicable for PM_{2.5}
33 studies.

34

35 **1 Introduction**

36 During the last decade, an extensive number of studies have researched the feasibility of
37 estimating PM_{2.5} (particulate matter with particle sizes smaller than 2.5 μm) pollution with the use
38 of passive-based satellite-derived aerosol optical depth (AOD; e.g., Liu et al., 2007; Hoff and
39 Christopher, 2009; van Donkelaar et al., 2015). Monitoring of PM concentration from space
40 observations is needed, as PM_{2.5} pollution is one of the known causes of respiratory related diseases
41 as well as other health related issues (e.g., Liu et al., 2005; Hoff and Christopher, 2009; Silva et
42 al., 2013). Yet, ground-based PM_{2.5} measurements are often inconsistent or have limited
43 availability over much of the globe.

44 In some earlier studies, empirical relationships of PM_{2.5} concentrations and AODs were
45 developed and used for estimating PM_{2.5} concentrations from passive sensor retrieved AODs (e.g.,
46 Wang and Christopher, 2003; Engel-Cox et al., 2004; Liu et al., 2005; Kumar et al., 2007; Hoff
47 and Christopher, 2009). One of the limitations of this approach is that vertical distributions and
48 thermodynamic state of aerosol particles vary with space and time. Especially for regions with
49 elevated aerosol plumes, deep boundary layer entrainment zones, or strong nighttime inversions,
50 column-integrated AODs are not a good approximation of surface PM_{2.5} concentrations at specific
51 points and times (e.g., Liu et al., 2004; Toth et al., 2014; Reid et al., 2017). Indeed, Kaku et al.
52 (2018) recently showed that surface PM_{2.5} had longer spatial correlation lengths than AOD, even
53 in the “well behaved” southeastern United States where previous studies showed good
54 performance (e.g., Wang and Christopher, 2003). To account for variability in aerosol vertical



55 distribution, several studies have attempted the use of chemical transport models, or CTMs (e.g.,
56 van Donkelaar et al., 2015). Satellite data assimilation of AOD has become commonplace, vastly
57 improving AOD analyses and short-term prediction (e.g., Zhang et al., 2014; Sessions et al., 2015).
58 Yet, PM_{2.5} simulations remain poor (e.g., Reid et al., 2016). Uncertainties in such studies are
59 unavoidable due to uncertainties in CTM-based aerosol vertical distributions, and no nighttime
60 AODs are currently available from passive-based satellite retrievals.

61 It is arguable that from a climatological/long-term average perspective, the use of AOD as
62 a proxy for PM_{2.5} concentrations nevertheless has certain qualitative skill (e.g., Toth et al., 2014;
63 Reid et al., 2017) for the most significant events as well as due to the averaging process that
64 suppresses sporadic aerosol events with highly variable vertical distributions. Still, as illustrated
65 in Fig. 1, where 2-year (2008-2009) means of Moderate Resolution Imaging Spectroradiometer
66 (MODIS) AOD are plotted against PM_{2.5} concentrations throughout the contiguous United States
67 (CONUS), although a linear relationship is plausibly shown, a low r^2 value of 0.09 is found. To
68 construct Fig. 1, Aqua MODIS Collection 6 (C6) Optical_Depth_Land_And_Ocean data (0.55
69 μm), restricted to “Very Good” retrievals as reported by the Land_Ocean_Quality_Flag, are first
70 collocated with daily surface PM_{2.5} measurements in both space and time (i.e., within 40 km in
71 distance and the same day), and then collocated daily pairs are averaged into 2-year means (for
72 each PM_{2.5} site). Figure 1 may be indicating that even from a long-term mean perspective, aerosol
73 vertical distributions are not uniform across the CONUS, which is also confirmed by other studies
74 (e.g., Toth et al., 2014). AOD retrievals themselves, with known uncertainties due to cloud
75 contamination and assumptions in the retrieval process (e.g., Levy et al., 2013), may also introduce
76 uncertainties to that task.



77 On board the Cloud-Aerosol Lidar and Infrared Pathfinder Satellite Observations
78 (CALIPSO) satellite, the Cloud-Aerosol Lidar with Orthogonal Polarization (CALIOP) instrument
79 provides observations of aerosol and cloud vertical distributions at both day and night (Hunt et al.,
80 2009; Winker et al., 2010). Given that CALIOP provides aerosol extinction retrievals near the
81 ground, it is interesting and reasonable to raise the question: can near surface CALIPSO extinction
82 be used as a better physical quantity than AOD for estimating surface $PM_{2.5}$ concentrations? This
83 is because unlike AOD, which is a column-integrated value, near surface CALIPSO extinction is,
84 in theory, a more realistic representation of near surface aerosol properties. Yet, in comparing
85 with passive sensors such as MODIS, which has a swath width on the order of ~ 2000 km, CALIOP
86 is a nadir pointing instrument with a narrow swath of ~ 70 m and a repeat cycle of 16 days (Winker
87 et al., 2009). Thus, the spatial sampling of CALIOP is sparse on a daily basis and temporal
88 sampling or other conditional or contextual biases are unavoidable if CALIOP observations are
89 used to estimate daily $PM_{2.5}$ concentrations (Zhang and Reid, 2009; Colarco et al., 2014). Also,
90 there are known uncertainties in CALIPSO retrieved extinction values due to uncertainties in the
91 retrieval process, such as the lidar ratio (extinction-to-backscatter ratio), calibration, and the
92 “retrieval fill value” (RFV) issue (Young et al., 2013; Toth et al., 2018).

93 Even with these known issues, especially the sampling bias, it is still compelling to
94 investigate if near surface CALIOP extinction can be utilized to retrieve surface $PM_{2.5}$
95 concentrations with reasonable accuracy from a long-term (i.e., two-year) mean perspective.
96 CALIOP data have been successfully used in $PM_{2.5}$ studies in the past, but primarily for assisting
97 passive-based AOD/ $PM_{2.5}$ analyses using aerosol vertical distribution as a constraint (e.g., Glantz
98 et al., 2009; van Donkelaar et al., 2010; Val Martin et al., 2013; Toth et al., 2014; Li et al., 2015;
99 Gong et al., 2017). However, the question remained as to the efficacy of the direct use of CALIOP



100 retrievals. To demonstrate a concept, we developed a bulk mass scattering scheme for inferring
101 PM concentrations from near surface aerosol extinction retrievals derived from CALIOP
102 observations. The bulk method used here is based upon the well-established relationship between
103 particle light scattering and PM_{2.5} aerosol mass concentration (e.g., Charlson et al., 1968;
104 Waggoner and Weiss, 1980; Liou, 2002; Chow et al., 2006), discussed further, with the relevant
105 equations, in Sect. 2.

106 In this study, using two years (2008-2009) of CALIOP and United States (U.S.)
107 Environmental Protection Agency (EPA) data over the CONUS, the following questions are
108 addressed:

- 109 1. Can CALIOP extinction be used effectively for estimating PM_{2.5} concentrations through a
110 bulk mass scattering scheme from a 2-year mean perspective for both daytime and
111 nighttime?
- 112 2. Can CALIOP extinction be used as a better parameter than AOD for estimating PM_{2.5}
113 concentrations from a 2-year mean perspective?
- 114 3. What are the sampling biases we can expect in CALIOP estimates of PM_{2.5}?
- 115 4. How do uncertainties in bulk properties compare to overall CALIOP-retrieved PM_{2.5}
116 uncertainty?

117 Details of the methods and datasets used are described in Sect. 2. Section 3 shows the
118 preliminary results using two years of EPA PM_{2.5} and CALIOP data, including an uncertainty
119 analysis. The conclusions of this paper are provided in Sect. 4.

120

121

122

123 **2 Data and Methods**

124 Since 1970, the U.S. EPA has monitored surface PM using a number of Federal
125 Reference/Equivalent Methods (FRMs/FEMs), which employ gravimetric, tapered element
126 oscillating microbalance (TEOM), and beta gauge instruments (Federal Register, 1997;
127 Greenstone, 2002). Two years (2008-2009) of daily PM_{2.5} Local Conditions (EPA code = 88101)
128 data were acquired from the EPA Air Quality System for use in this investigation, consistent with
129 our previous PM_{2.5} study (Toth et al., 2014). We note that these data represent PM_{2.5} concentrations
130 over a 24-hour period and include two scenarios: one sample is taken during the 24-hour duration
131 (i.e., filter-based measurement), or an average is computed from hourly samples within this time
132 period (every hour may not have an available measurement, however).

133 CALIOP, flying aboard the CALIPSO platform within the A-Train satellite constellation,
134 is a dual wavelength (0.532 and 1.064 μm) lidar that has collected profiles of atmospheric aerosol
135 particles and clouds since summer 2006 (Winker et al., 2007). In this study, daytime and nighttime
136 extinction coefficients retrieved at 0.532 μm from the Version 4.10 CALIOP Level 2 5 km aerosol
137 profile (L2_05kmAPro) product were used. Using parameters provided in the L2_05kmAPro
138 product, as well as the corresponding Level 2 5 km aerosol layer (L2_05kmALay) product, a robust
139 quality-assurance (QA) procedure for the aerosol observations was implemented (Table 1).
140 Further information on the QA metrics and screening protocol are discussed in detail in previous
141 studies (Kittaka et al. 2011; Campbell et al. 2012; Toth et al. 2013; 2016). Once the QA procedure
142 was applied, the aerosol profiles were linearly re-gridded from 60 m vertical resolution (above
143 mean sea level [AMSL]) to 100 m segments (i.e., resampled to 100 m resolution) referenced to the
144 local surface (above ground level [AGL]; Toth et al., 2014; 2016). The choice of 100 m was
145 arbitrary, and the profiles were re-gridded in order to obtain an AGL-corrected dataset, as opposed



146 to the AMSL-referenced profiles provided by the L2_05kmAPro product. Surface elevation and
147 relative humidity (RH) were taken from collocated model data included in the CALIPSO
148 L2_05kmAPro product (CALIPSO Data Products Catalog (Release 4.20); RH taken from the
149 Modern Era Retrospective-Analysis for Research, or MERRA-2 reanalysis product). To limit the
150 effects of signal attenuation and increase the chances of measuring aerosol presence near the
151 surface, the Atmospheric Volume Description parameter within the L2_05kmAPro dataset is used
152 to cloud-screen each aerosol profile as in Toth et al. (2018).

153 In this study, near surface PM mass concentration (C_m) is derived from near surface
154 CALIOP extinction based on a bulk formulation as in Equation 1 (e.g., Liou, 2002; Chow et al.,
155 2006):

$$156 \quad \beta = C_m(a_{scat}f_{rh} + a_{abs}) \times 1000 \quad (1)$$

157 where β is CALIOP-derived near surface extinction in km^{-1} , C_m is the PM mass
158 concentration in $\mu\text{g m}^{-3}$, a_{scat} and a_{abs} are dry mass scattering and absorption efficiencies in $\text{m}^2 \text{g}^{-1}$,
159 and f_{rh} represents the light scattering hygroscopicity, respectively. As a preliminary study, for the
160 purpose of demonstrating this concept, we assume the dominant aerosol type over the contiguous
161 U.S. (CONUS) is pollution aerosol (i.e., the most prevalent near-surface aerosol type reported in
162 the CALIOP products for the CONUS during 2008-2009 is polluted continental) with a_{scat} and a_{abs}
163 values of 3.40 and $0.37 \text{ m}^2 \text{g}^{-1}$ (Hess et al., 1998; Lynch et al., 2016), respectively. These values
164 are similar to those reported in Malm and Hand (2007) and Kaku et al. (2018) but are interpolated
165 to $0.532 \mu\text{m}$ from values at $0.450 \mu\text{m}$ and $0.550 \mu\text{m}$ obtained from the Optical Properties of
166 Aerosols and Clouds (OPAC) model (Hess et al., 1998). Still, both a_{scat} and a_{abs} have regional and
167 species related dependencies. Also, only 2-year averages are used in this study, and we assume
168 that sporadic aerosol plumes are smoothed out in the averaging process, and that bulk aerosol



169 properties are similar throughout the study region. We have further explored the impact of aerosol
170 types to $PM_{2.5}$ retrievals in a later section. Furthermore, to aid in focusing this study on fine
171 mode/anthropogenic aerosols, those aerosol extinction range bins classified as dust by the CALIOP
172 typing algorithm were excluded from the analysis.

173 Also, surface PM concentrations are dry mass measurements. To account for the impact
174 of humidity on a_{scat} (it is assumed that a_{abs} is not affected by moisture), we estimated the
175 hygroscopic growth factor for pollution aerosol based on Hanel (1976), as shown in Equation 2:

$$176 \quad f_{rh} = \left(\frac{1 - RH}{1 - RH_{ref}} \right)^{-\Gamma} \quad (2)$$

177 where f_{rh} is the hygroscopic growth factor, RH is the relative humidity, and RH_{ref} is the
178 reference RH and is set to 30% in this study (Lynch et al., 2016). Γ is a unitless value (a fit
179 parameter describing the amount of hygroscopic increase in scattering) and is assumed to be 0.63
180 (i.e., sulfate aerosol) in this study (Hanel, 1976; Chew et al., 2016; Lynch et al., 2016).

181 Lastly, the CALIOP-derived PM density is for all particle sizes. To convert from mass
182 concentration of PM (C_m) to mass concentration of $PM_{2.5}$ ($C_{m2.5}$), which represents mass
183 concentration for particle sizes smaller than 2.5 μm , we adopted the $PM_{2.5}$ to PM_{10} (PM with
184 diameters less than 10 μm) ratio (ϕ) of 0.6 as measured during the Studies of Emissions and
185 Atmospheric Composition, Clouds and Climate Coupling by Regional Surveys (SEAC⁴RS)
186 campaign over the US (Kaku et al., 2018). Again, the ratio of $PM_{2.5}$ to PM_{10} can also vary spatially,
187 however we used a regional mean to demonstrate the concept. Analyses in a later section using
188 two-years (2008-2009) of surface $PM_{2.5}$ to PM_{10} data suggest that 0.6 is a rather reasonable number
189 to use for the CONUS for the study period. Here we assume that mass concentrations for particle
190 sizes larger than 10 μm are negligible over the CONUS. Thus, we can rewrite Equation 1 as:



$$C_{m2.5} = \frac{\beta \times \phi}{(a_{scat} \times f_{rh} + a_{abs}) \times 1000} \quad (3)$$

where $C_{m2.5}$ is the CALIOP-derived $PM_{2.5}$ concentration in units of $\mu g m^{-3}$.

193

194 **3 Results and Discussion**

195 **3.1 Regional analysis**

196 Figure 2a shows the mean $PM_{2.5}$ concentration using two years (2008-2009) of daily
197 surface $PM_{2.5}$ data from the U.S. EPA ($PM_{2.5_EPA}$), not collocated with CALIOP observations. A
198 total of 1,091 stations (some operational throughout the entire period; others only partially) are
199 included in the analysis and observations from those stations are further used in evaluating
200 CALOP-derived $PM_{2.5}$ concentrations ($C_{m2.5}$), as later shown in Fig. 3. $PM_{2.5}$ concentrations of
201 $\sim 10 \mu g m^{-3}$ are found over the eastern CONUS. In comparison, much lower $PM_{2.5}$ concentrations
202 of $\sim 5 \mu g m^{-3}$ are exhibited for the interior CONUS, over states including Montana, Wyoming,
203 North Dakota, South Dakota, Utah, Colorado, and Arizona. For the west coast of the CONUS,
204 and especially over California, higher $PM_{2.5}$ concentrations are observed, with the maximum two-
205 year mean near $20 \mu g m^{-3}$. Note that the spatial distribution of surface $PM_{2.5}$ concentrations over
206 the CONUS as shown in Fig. 2a is consistent with reported values from several studies (e.g., Hand
207 et al., 2013; Van Donkelaar et al., 2015; Di et al., 2017).

208 Figure 3a shows the two-year averaged $1^\circ \times 1^\circ$ (latitude/longitude) gridded daytime
209 CALIOP aerosol extinction over the CONUS using CALIOP observations from 100-1000 m,
210 referenced to the number of cloud-free L2_05kmAPro profiles in each $1 \times 1^\circ$ bin. The lowest 100
211 m of CALIOP extinction data are not used in the analysis due to the potential of surface return
212 contamination (e.g., Toth et al., 2014), although this has been improved for the Version 4 CALIOP
213 products but may still be present in some cases. Here the averaged extinction from 100-1000 m is



214 used to represent near surface aerosol extinction. This selection of the 100-1000 m layer is
215 somewhat arbitrary, even though it is estimated from the mean CALIOP-based aerosol vertical
216 distribution over the CONUS (Toth et al., 2014), as surface layer heights may change seasonally
217 and diurnally. Thus, a sensitivity study is provided in a later section to understand the impact of
218 this aerosol layer selection to CALIOP-based $PM_{2.5}$ retrievals. As shown in Fig. 3a, higher mean
219 near surface CALIOP extinction of 0.1 km^{-1} are found for the eastern CONUS and over California,
220 while lower values of $0.025\text{-}0.05 \text{ km}^{-1}$ found for the interior CONUS. Figure 3b shows a plot
221 similar to Fig. 3a but using nighttime CALIOP observations only. Although similar spatial
222 patterns are found during both day and night, the near surface extinction values are overall lower
223 for nighttime than daytime, and nighttime data are less noisy than daytime. These findings are not
224 surprising, as daytime CALIOP measurements are subject to contamination from background solar
225 radiation (e.g., Omar et al., 2013).

226 To investigate any diurnal biases in the data, Figs. 3c and 3d show the derived $PM_{2.5}$
227 concentration using daytime and nighttime CALIOP data respectively, based on the method
228 described in Section 2. Both Figures 3c and 3d suggest a higher $PM_{2.5}$ concentration of $\sim 10\text{-}12.5$
229 $\mu\text{g m}^{-3}$ over the eastern CONUS, and a much lower $PM_{2.5}$ concentration of $\sim 2.5\text{-}5 \mu\text{g m}^{-3}$ over the
230 interior CONUS. High $PM_{2.5}$ values of $10\text{-}20 \mu\text{g m}^{-3}$ are also found over the west coast of the
231 CONUS, particularly over California. The spatial distribution of $PM_{2.5}$ concentrations, as derived
232 using near surface CALIOP data (Figs. 3c and 3d, as well as the combined daytime and nighttime
233 perspective shown in Fig. 2c), is remarkably similar to the spatial distribution of $PM_{2.5}$ values as
234 estimated based on ground-based observations (Fig. 2a). Still, day and night differences in $PM_{2.5}$
235 concentrations are also clearly visible, as higher $PM_{2.5}$ values are found, in general, during daytime,
236 based on CALIOP observations. The high daytime $PM_{2.5}$ values, as shown in Fig. 3c, may



237 represent stronger near surface convection and more frequent anthropogenic activities during
238 daytime. However, they may also be partially contributed from solar radiation contamination.
239 Another possibility is that the daytime mean extinction coefficients (from which the mean $PM_{2.5}$
240 estimates are derived) appear artificially larger than at night due to high daytime noise limiting the
241 ability of CALIOP to detect fainter aerosol layers during daylight operations.

242 Figure 3e shows the inter-comparison between $PM_{2.5_EPA}$ and $PM_{2.5_CALIOP}$ concentrations.
243 Note that only CALIOP and ground-based $PM_{2.5}$ data pairs, which are within 100 km of each other
244 and have reported values for the same day (i.e., year, month, and day), are used to generate Fig.
245 3e. Still, although only spatially and temporally collocated data pairs are used, ground-based $PM_{2.5}$
246 data represent 24-hour averages, while CALIOP-derived $PM_{2.5}$ concentrations are instantaneous
247 values over the daytime CALIOP overpass. To reduce this temporal bias, two years (2008-2009)
248 of collocated CALIOP-derived and measured $PM_{2.5}$ concentrations are averaged and only the two-
249 year averages are used in constructing Fig 3e. Also, to minimize the above-mentioned temporal
250 sampling bias, ground stations with fewer than 100 collocated pairs are discarded. This leaves a
251 total of 276 stations for constructing Fig. 3e.

252 As shown in Fig. 3e, an r^2 value of 0.21 (with a slope of 0.48) is found between CALIOP-
253 derived and measured surface $PM_{2.5}$ concentrations, with a corresponding mean bias of $-0.40 \mu g$
254 m^{-3} ($PM_{2.5_CALIOP} - PM_{2.5_EPA}$). In comparison, Fig. 3f shows results similar to Fig. 3e, but for
255 nighttime CALIOP data. A much higher r^2 value of 0.48 (with a slope of 0.67) is found between
256 CALIOP-derived and measurement $PM_{2.5}$ values from 528 EPA stations, with a corresponding
257 mean bias of $-3.3 \mu g m^{-3}$ ($PM_{2.5_CALIOP} - PM_{2.5_EPA}$). This may be related to the diurnal variability
258 of $PM_{2.5}$ concentrations, as the daily mean EPA measurement might be closer to the CALIOP A.M.
259 retrieval than to its P.M. counterpart. Still, data points are more scattered in Fig. 3e in comparison



260 with Fig. 3f, which again indicates that daytime CALIOP data are noisier, possibly due to daytime
261 solar contamination as well as other factors such as biases in relative humidity. Details of these
262 biases are further explored in Section 3.2.

263 To supplement this analysis, a pairwise $PM_{2.5_EPA}$ and $PM_{2.5_CALIOP}$ (day and night CALIOP
264 combined) analysis is presented in the spatial plots of Figs. 2b and 2d. Here, however, we lift the
265 100 collocated pairs requirement to increase data samples for better spatial representativeness. The
266 spatial variability of $PM_{2.5}$ over the CONUS is consistent with the observed patterns of non-
267 collocated data (i.e., Figs. 2a and 2c), but with generally higher values due to differences in
268 sampling. Also, comparing Figs. 2b and 2d, $PM_{2.5_EPA}$ spatial patterns match well with those of
269 $PM_{2.5_CALIOP}$, yet with larger values for $PM_{2.5_EPA}$ (consistent with the biases discussed above).
270 Lastly, a scatterplot of the pairwise analysis shown in Figs. 2b and 2d is provided in Fig. 4. An r^2
271 value of 0.40 is found between EPA and CALIOP-derived $PM_{2.5}$ concentrations from a combined
272 daytime and nighttime CALIOP perspective. Overall, Figs. 2, 3, and 4 indicate that near surface
273 CALIOP extinction data can be used to estimate surface $PM_{2.5}$ concentrations with reasonable
274 accuracy.

275

276 3.2 Uncertainty analysis

277 In this section, uncertainties in the CALIOP derived, 2-year averaged $PM_{2.5}$ concentrations
278 are explored as functions of aerosol vertical distribution, $PM_{2.5}$ to PM_{10} ratio, RH, aerosol type,
279 and cloud presence above. Spatial sampling related biases as well as prognostic errors are also
280 studied.

281

282



283 3.2.1 Prognostic errors in $C_{m2.5}$

284 As a first step for the uncertainty analysis, we estimated the prognostic error of 2-year
285 averaged $PM_{2.5_CALIOP}$. Figure 5 shows the root-mean-square error (RMSE) of CALIOP-based
286 $PM_{2.5}$ concentrations against those from EPA stations as a function of CALIOP-based $PM_{2.5}$ for
287 the 2008-2009 period over the CONUS. RMSEs were computed in intervals of $5 \mu g m^{-3}$ from 0
288 to $25 \mu g m^{-3}$, with no computations greater than $25 \mu g m^{-3}$ performed due to very few data points
289 above this $PM_{2.5}$ concentration level. A mean combined daytime and nighttime minimum error of
290 $\sim 4 \mu g m^{-3}$ is found, with generally larger RMSEs for nighttime below $15 \mu g m^{-3}$, and larger RMSEs
291 for daytime above $15 \mu g m^{-3}$. However, mean RMSEs (i.e., computed from the RMSEs shown in
292 Fig. 5) are similar for both datasets, $\sim 4.5 \mu g m^{-3}$ for daytime and $\sim 4.0 \mu g m^{-3}$ for nighttime. Also,
293 note that while the absolute error for daytime is largest at high $PM_{2.5}$ concentrations, relative errors
294 are similar (e.g., $3 \mu g m^{-3}/10 \mu g m^{-3}$ or 30% for the $5\text{-}10 \mu g m^{-3}$ bin, versus $7 \mu g m^{-3}/25 \mu g m^{-3}$ or
295 28% for the $20\text{-}25 \mu g m^{-3}$ bin). For context, the number of samples per bin are also plotted (as X
296 symbols) in Fig. 5. Data sample sizes are smallest (largest) for the lowest/highest range (mid-
297 range) $PM_{2.5}$ bins.

298

299 3.2.2 Surface layer height sensitivity study

300 A sensitivity study was conducted for which $PM_{2.5}$ was derived from near-surface CALIOP
301 aerosol extinction by varying the height of the surface layer in increments of 100 m from the
302 ground to 1000 m. Note that the surface layer (0-100 m) is included for this sensitivity study only.
303 The statistical results of this analysis, for both daytime and nighttime conditions, are shown in
304 Table 2. Four statistical parameters were computed, consisting of r^2 , slope, mean bias (CALIOP
305 – EPA) of $PM_{2.5}$, and percent error change in derived $PM_{2.5}$, defined as: $((\text{mean_new_}PM_{2.5} -$



306 $\text{mean_original_PM}_{2.5})/\text{mean_original_PM}_{2.5}) * 100$. For context, the bottom row of Table 2 shows
307 the results from the original analysis. In terms of r^2 and slope, optimal values peak at different
308 surface layer heights between daytime and nighttime. For example, for daytime, the largest
309 correlations are found for the 0-600 m and 0-700 m layers, while for nighttime these are found for
310 the 0-300 m and 0-400 m layers. However, the 0-300 m layer (100-1000 m layer) exhibits the
311 lowest mean bias for the daytime (nighttime) analysis. Overall, marginal changes are found for
312 varying the height of the surface layer. Yet the largest mean bias is found for the 0-100 m layer,
313 indicating the need for excluding the 0-100 m layer in the analysis.

314

315 **3.2.3 RH sensitivity study**

316 Profiles of RH were taken from the MERRA-2 reanalysis product, as these collocated data
317 are provided in the CALIPSO L2_05kmAPro product. However, biases may exist in this RH
318 dataset. Thus, we examined the impact of varying the RH values by +/- 10% on the CALIOP-
319 derived $\text{PM}_{2.5}$ concentrations. For both daytime and nighttime analyses, no significant differences
320 in the r^2 and slope values were found. However, a +15% (-15%) change in the mean derived $\text{PM}_{2.5}$
321 values was found by decreasing (increasing) the RH values by 10%.

322

323 **3.2.4 $\text{PM}_{2.5}$ to PM_{10} ratio sensitivity study**

324 Another source of uncertainty in this study is the $\text{PM}_{2.5}/\text{PM}_{10}$ ratio. Using surface-based
325 $\text{PM}_{2.5}$ and PM_{10} data from those EPA stations over the CONUS for 2008-2009 with concurrent
326 $\text{PM}_{2.5}$ and PM_{10} daily data available (i.e., 409 stations), we computed the mean $\text{PM}_{2.5}/\text{PM}_{10}$ ratio,
327 and its corresponding standard deviation. The mean ratio was 0.56 with a standard deviation of
328 0.32. It is interesting to note that the mean $\text{PM}_{2.5}/\text{PM}_{10}$ ratio estimated from two years of surface



329 observations over the CONUS is close to 0.6 (the number used in this study), as reported by Kaku
330 et al. (2018). We also tested the sensitivity of the derived $PM_{2.5}$ concentrations as a function of
331 $PM_{2.5}/PM_{10}$ ratio for two scenarios: ± 1 standard deviation of the mean (Table 3). In general, a ± 50
332 % to 60 % change is found with the variation of the $PM_{2.5}/PM_{10}$ ratio at the range of ± 1 standard
333 deviation of the mean. As suggested from Table 3, the optimal slope is found using a ratio of $+1$
334 standard deviation of the mean for both daytime and nighttime. The lowest mean daytime bias is
335 found for a ratio of 0.6, and for nighttime the lowest mean bias occurs using a ratio of 0.88.

336

337 **3.2.5 Sampling-related biases**

338 As mentioned in the introduction section, a sampling bias, due to the very small footprint
339 size and ~ 16 day repeat cycle of CALIOP, can exist when using CALIOP observations for $PM_{2.5}$
340 estimates (Zhang and Reid, 2009). This sampling-induced bias is investigated from a 2-year mean
341 perspective by comparing histograms of $PM_{2.5_EPA}$ and $C_{m2.5}$ concentrations as shown in Fig. 6. To
342 generate Fig. 6, all available daily EPA $PM_{2.5}$ are used to represent the “true” 2-year mean spectrum
343 of $PM_{2.5}$ concentrations over the EPA sites. The aerosol extinction data spatially collocated to the
344 EPA sites (Sect. 3.1), but not temporally collocated, are used for estimating the 2-year mean
345 spectrum of $PM_{2.5}$ concentrations as derived from CALIOP observations. To be consistent with
346 the previous analysis, only cloud-free CALIOP profiles are considered. The $PM_{2.5_EPA}$
347 concentrations peak at $\sim 9 \mu g m^{-3}$ (standard deviation of $\sim 3 \mu g m^{-3}$), and CALIOP-derived $PM_{2.5}$
348 peaks at $\sim 9 \mu g m^{-3}$ (daytime; standard deviation of $\sim 4 \mu g m^{-3}$) and $\sim 5 \mu g m^{-3}$ (nighttime; standard
349 deviation of $\sim 2 \mu g m^{-3}$). The distribution shifts towards smaller concentrations for CALIOP, more
350 so for nighttime than daytime (possibly due to CALIOP daytime versus nighttime detection
351 differences).



352 Still, Fig. 6 may reflect the diurnal difference in $PM_{2.5}$ concentrations as well as the
353 retrieval bias in $C_{m2.5}$ values. Thus, we have re-performed the exercise shown in Fig. 6 using
354 spatially and temporally collocated $PM_{2.5_EPA}$ and $C_{m2.5}$ data as shown in Fig. 7. To construct Fig.
355 7, $PM_{2.5_EPA}$ and $C_{m2.5}$ data are collocated following the steps mentioned in Sect. 3.1, with CALIOP
356 and EPA $PM_{2.5}$ representing 2-year mean values for each EPA station. Again, only cloud-free
357 CALIOP profiles are considered for this analysis. As shown in Fig. 7a, the $PM_{2.5_EPA}$
358 concentrations peak at $\sim 7 \mu\text{g m}^{-3}$ (standard deviation of $\sim 4 \mu\text{g m}^{-3}$), and daytime $C_{m2.5}$ peaks at
359 $\sim 6 \mu\text{g m}^{-3}$ (standard deviation of $\sim 4 \mu\text{g m}^{-3}$). In comparison, with the use of collocated nighttime
360 $C_{m2.5}$ and $PM_{2.5_EPA}$ data as shown in Fig. 7b, the peak $PM_{2.5_EPA}$ value is about $2 \mu\text{g m}^{-3}$ higher
361 than the peak $C_{m2.5}$ value (with similar standard deviations as found in the analyses of Fig. 7a).
362 Considering both Figs. 6 and 7, it is likely that the temporal sampling bias seen in Fig. 6 is at least
363 in part due to retrieval bias as well as the difference in $PM_{2.5}$ concentrations during daytime and
364 nighttime.

365

366 3.2.6 CALIOP AOD analysis

367 Most past studies focused on the use of column AODs as proxies for surface $PM_{2.5}$ (e.g.,
368 Liu et al., 2005; Hoff and Christopher, 2009; van Donkelaar et al., 2015). Therefore, it is
369 interesting to investigate whether near surface CALIOP extinction values can be used as a better
370 physical quantity to estimate surface $PM_{2.5}$ in comparing with column-integrated CALIOP AOD.
371 To achieve this goal, we have compared CALIOP column AOD and $PM_{2.5}$ from EPA stations, as
372 shown in Fig. 8. Similar to the scatterplots of Fig. 4, each point represents a two-year mean for
373 each EPA site, and was created from a dataset following the same spatial/temporal collocation as
374 described above. As shown in Fig. 9, r^2 values of 0.04 and 0.13 are found using CALIOP daytime



375 and nighttime AOD data, respectively, similar to the MODIS-based analysis shown in Fig. 1. This
376 is expected, as elevated aerosol layers will negatively impact the relationship between surface
377 $PM_{2.5}$ and column AOD. The derivation of surface $PM_{2.5}$ from near surface CALIOP extinction,
378 as demonstrated from this study however, provides a much better spatial matching between the
379 quantities being compared, with potential error terms that can be well quantified and minimized in
380 later studies.

381

382 **3.2.7 Cloud flag sensitivity study**

383 For most of this paper, a strict cloud screening process is implemented, during which no
384 clouds are allowed in the entire CALIOP profile. However, in contrast to passive sensor
385 capabilities (e.g., MODIS), near-surface aerosol extinction coefficients can be readily retrieved
386 from CALIOP profiles even when there are transparent cloud layers above. Therefore, we
387 conducted an additional analysis for which no cloud flag was set (i.e., all-sky conditions). Results
388 are shown in scatterplot form in Fig. 9, in a similar manner as Figs. 3e and f, with an additional 97
389 (156) points for the daytime (nighttime) analyses. Comparing the all-sky results with those of
390 Figs. 3e, and f (cloud-free conditions), the r^2 values are similar. This is also true in terms of mean
391 bias, with similar values of 0.70 (-2.68) $\mu\text{g m}^{-3}$ found for daytime (nighttime) for all-sky scenarios.
392 This indicates that our method performs reasonably well from an all-sky perspective. However,
393 we note that restricting the analysis to solely those cases that are cloudy (not shown), the method
394 does not perform as well. For example, the r^2 values decrease by 71% (90%) and the slope values
395 decrease by 21% (75%) for the daytime (nighttime) analyses, compared to the cloud-free results
396 (Figs. 3e and f). This is expected, as any errors made in estimating the optical depths of the



397 overlying clouds will propagate (as biases) into the extinction retrievals for the underlying
398 aerosols.

399

400 **3.2.8 Aerosol type analysis**

401 Also, for this study, we assume that the primary aerosol type over the CONUS is pollution
402 (i.e., sulfate & organic) aerosol, which is generally composed of smaller (fine mode) particles that
403 tend to exhibit mass extinction efficiencies $\sim 4 \text{ m}^2 \text{ g}^{-1}$. However, even after implementing our dust-
404 free restriction, the study region can also be contaminated with non-pollution aerosols, which can
405 have a larger particle size and exhibit lower mass extinction efficiencies (e.g., Hess et al., 1998;
406 Malm and Hand, 2007; Lynch et al., 2016). The use of $\text{PM}_{2.5}$ versus PM_{10} somewhat mitigates
407 this size dependency, but nevertheless coarse mode dust or sea salt can dominate $\text{PM}_{2.5}$ mass values
408 (e.g., Atwood et al., 2013).

409 Thus, in this section, the impact of aerosol types to the derived $\text{PM}_{2.5}$ concentrations was
410 explored by varying the mass scattering and absorption efficiencies and gamma values associated
411 with each aerosol type. The three aerosol types chosen for this sensitivity study were dust, sea
412 salt, and smoke, based upon Lynch et al. (2016). The mass scattering and absorption values for
413 dust and sea salt were interpolated to $0.532 \mu\text{m}$ from values at $0.450 \mu\text{m}$ and $0.550 \mu\text{m}$ from OPAC
414 (as was done for the sulfate case; Hess et al., 1998). For smoke, these values were interpolated to
415 $0.532 \mu\text{m}$ from values at $0.440 \mu\text{m}$ and $0.670 \mu\text{m}$ as provided by Reid et al. (2005) for smoke cases
416 over the US and Canada. The gamma values were taken from Lynch et al. (2016) and the
417 references within. These values, as well as the results from this sensitivity study, are shown in
418 Table 4. If we assume all aerosols within the study region are smoke aerosols, no major changes
419 in the retrieved CALIOP $\text{PM}_{2.5}$ values are found. However, significant uncertainties on the order



420 of ~200% (~800%) are found if sea salt (dust) aerosol mass scattering/absorption efficiencies and
421 gamma values are used instead. Clearly, this study suggests that accurate aerosol typing is
422 necessary for future applications of CALIOP observations for surface PM_{2.5} estimations.

423

424 **3.2.9 E-folding correlation length for PM_{2.5} concentrations over the CONUS**

425 As a last study, we also estimated the spatial e-folding correlation length for PM_{2.5}
426 concentrations over the CONUS. This provides us an estimation of the correlation between a
427 CALIOP-derived and actual PM_{2.5} concentration for a given location as a function of distance
428 between the CALIOP observation and the given location. To accomplish this, for 2008-2009 over
429 the CONUS, the distances and correlations (of PM_{2.5} concentration) were computed for any two
430 EPA stations with over 50 days of daily data for the two-year period. Results are shown in Fig.
431 10 as a scatterplot, with individual points in gray and the black curve representing the exponential
432 fit to the data. A decrease in PM_{2.5} correlation with distance between EPA stations is found, and
433 the e-folding length in correlation (e.g., correlation reduced to 1/e, or 0.37) is ~600 km (from an
434 AOD standpoint, this value is 40-400 km, as suggested by Anderson et al., 2003).

435 Also included in Fig. 10 are results from a corresponding regional analysis, with the red
436 and blue lines showing bin averages (10 km) for the Western and Eastern CONUS, respectively
437 (regions partitioned by the -97° longitude line). The e-folding length is ~300 km (~700 km) for
438 the Western (Eastern) CONUS, indicating a much shorter correlation length for pollution over the
439 Western CONUS, possibly due to a more complex terrain such as mountains. Overall these PM_{2.5}
440 e-folding lengths suggest that CALIOP-derived PM_{2.5} concentrations could still have some
441 representative skill within a few hundred kilometers of a given location.

442

443 **4 Conclusions**

444 In this paper, we have demonstrated a new bulk-mass-modeling method for retrieving
445 surface particulate matter (PM) with particle sizes smaller than $2.5\ \mu\text{m}$ ($\text{PM}_{2.5}$) using observations
446 acquired by the NASA Cloud-Aerosol Lidar with Orthogonal Polarization (CALIOP) instrument
447 from 2008-2009. For the purposes of demonstrating this concept, only regionally-averaged
448 parameters, such as mass scattering and absorption coefficients, and $\text{PM}_{2.5}$ to PM_{10} (PM with
449 particle sizes smaller than $10\ \mu\text{m}$) conversion ratio, are used. Also, we assume the dominant type
450 of aerosols over the study region is pollution aerosols (supported by the occurrence frequencies of
451 aerosol types determined by the CALIOP algorithms), and exclude aerosol extinction range bins
452 classified as dust from the analysis. Even with the highly-averaged parameters, the results from
453 this paper are rather promising and demonstrate a potential for monitoring PM pollution using
454 active-based lidar observations. Specifically, the primary results of this study are as follows:

- 455 1. CALIOP-derived $\text{PM}_{2.5}$ concentrations of $\sim 10\text{-}12.5\ \mu\text{g m}^{-3}$ are found over the eastern
456 contiguous United States (CONUS), with lower values of $\sim 2.5\text{-}5\ \mu\text{g m}^{-3}$ over the central
457 CONUS. $\text{PM}_{2.5}$ values of $\sim 10\text{-}20\ \mu\text{g m}^{-3}$ are found over the west coast of the CONUS,
458 primarily California. The spatial distribution of 2-year mean $\text{PM}_{2.5}$ concentrations derived
459 from near surface CALIOP aerosol data compares well to the spatial distribution of *in situ*
460 $\text{PM}_{2.5}$ measurements collected at the ground-based stations of the U.S. Environmental
461 Protection Agency (EPA). The use of nighttime CALIOP extinction to derive $\text{PM}_{2.5}$ results
462 in a higher correlation ($r^2 = 0.48$; mean bias = $-3.3\ \mu\text{g m}^{-3}$) with EPA $\text{PM}_{2.5}$ than daytime
463 CALIOP extinction data ($r^2 = 0.21$; mean bias = $-0.40\ \mu\text{g m}^{-3}$).
- 464 2. Correlations between CALIOP aerosol optical depth (AOD) and EPA $\text{PM}_{2.5}$ are much
465 lower (r^2 values of 0.04 and 0.13, for daytime and nighttime CALIOP AOD data,



466 respectively) than those obtained from derived $PM_{2.5}$ using near-surface CALIOP aerosol
467 extinction. A similar correlation is also found between Moderate Resolution Imaging
468 Spectroradiometer (MODIS) AOD and EPA $PM_{2.5}$ from two-year (2008-2009) means.
469 This suggests that CALIOP extinction may be used as a better parameter for estimating
470 $PM_{2.5}$ concentrations from a 2-year mean perspective. Also, the algorithm proposed in this
471 study is essentially a semi-physical-based method, and thus the retrieval process can be
472 improved, upon a careful study of the physical parameters used in the process.

473 3. Spatial and temporal sampling biases, as well as a retrieval bias, are found. Also, several
474 sensitivity studies were conducted, including surface layer height, cloud flag, $PM_{2.5}/PM_{10}$
475 ratio, relative humidity, and aerosol type. The sensitivity studies highlight the need for
476 accurate aerosol typing for estimating $PM_{2.5}$ concentrations using CALIOP observations.
477 4. Using surface-based $PM_{2.5}$ at EPA stations alone, the e-folding correlation length for $PM_{2.5}$
478 concentrations was found to be about 600 km for the CONUS. A regional analysis yielded
479 values of ~ 300 km and ~ 700 km for the Western and Eastern CONUS, respectively. Thus,
480 while limited in spatial sampling, measurements from CALIOP may still be used for
481 estimating $PM_{2.5}$ concentrations over the CONUS.

482 As noted earlier, CALIOP observations are still rather sparse, and concerns related to
483 reported CALIOP aerosol extinction values also exist, such as solar and surface contamination and
484 the “retrieval fill value” issue (e.g., Toth et al., 2018). Yet, the future High Spectral Resolution
485 Lidar (HSRL) instrument on board the Earth Clouds, Aerosol, and Radiation Explorer
486 (EarthCARE) satellite (Illingworth et al., 2015), as well as forthcoming space-based lidar missions
487 in response to the 2017 Decadal Survey, offer opportunities to further explore aerosol extinction -



488 based PM concentrations. Ultimately the results from this study show that the combined use of
489 several lidar instruments for monitoring regional and global PM pollution is potentially achievable.

490

491

492

493

494

495

496

497

498

499

500

501

502

503

504

505

506

507

508

509

510



511 **Acknowledgements**

512 This research was funded with the support of the NASA Earth and Space Science Fellowship
513 program (NNX16A066H). Author JZ acknowledges the support from NASA grant
514 NNX17AG52G. CALIPSO data were obtained from the NASA Langley Research Center
515 Atmospheric Science Data Center (eos-web.larc.nasa.gov). MODIS data were obtained from
516 NASA Goddard Space Flight Center (ladsweb.nascom.nasa.gov). The PM_{2.5} data were obtained
517 from the EPA AQS site (https://aq5.epa.gov/aqsweb/airdata/download_files.html).

518

519

520

521

522

523

524

525

526

527

528

529

530

531



532 **References**

533

- 534 Anderson, T.L., Charlson, R. J., Winker, D.M., Ogren, J.A., and Holmén, K.: Mesoscale
535 Variations of Tropospheric Aerosols, *J. Atmos. Sci.*, 60, 119–136,
536 [https://doi.org/10.1175/1520-0469\(2003\)060<0119:MVOTA>2.0.CO;2](https://doi.org/10.1175/1520-0469(2003)060<0119:MVOTA>2.0.CO;2), 2003.
- 537 Atwood, S. A., J. S. Reid, S. M. Kreidenweis, S. S. Cliff, Y. Zhao, N.-H. Lin, S.-C. Tsay, Y.-C.
538 Chu, and Westphal, D.L.: Size resolved measurements of springtime aerosol particles over
539 the northern South China Sea, *Atmospheric Environment*, 78, 134-143,
540 <https://doi.org/10.1016/j.atmosenv.2012.11.024>, 2013.
- 541 Campbell, J. R., Tackett, J. L., Reid, J. S., Zhang, J., Curtis, C. A., Hyer, E. J., Sessions, W. R.,
542 Westphal, D. L., Prospero, J. M., Welton, E. J., Omar, A. H., Vaughan, M. A., and Winker,
543 D. M.: Evaluating nighttime CALIOP 0.532 μm aerosol optical depth and extinction
544 coefficient retrievals, *Atmos. Meas. Tech.*, 5, 2143-2160, [https://doi.org/10.5194/amt-5-](https://doi.org/10.5194/amt-5-2143-2012)
545 [2143-2012](https://doi.org/10.5194/amt-5-2143-2012), 2012.
- 546 Charlson, R. J., Ahlquist, N. C., and Horvath, H.: On the generality of correlation of atmospheric
547 aerosol mass concentration and light scatter, *Atmospheric Environment*, 2(5), 455-464,
548 [https://doi.org/10.1016/0004-6981\(68\)90039-5](https://doi.org/10.1016/0004-6981(68)90039-5), 1968.
- 549 Chew, B. N., Campbell, J. R., Hyer, E. J., Salinas, S. V., Reid, J. S., Welton, E. J., Holben, B.N.
550 and Liew, S. C.: Relationship between aerosol optical depth and particulate matter over
551 Singapore: Effects of aerosol vertical distributions, *Aerosol and Air Quality Research*, 16,
552 2818-2830, <https://doi.org/10.4209/aaqr.2015.07.0457>, 2016.
- 553 Chow, J. C., Watson, J. G., Park, K., Robinson, N. F., Lowenthal, D. H., Park, K., and Magliano,
554 K. A.: Comparison of particle light scattering and fine particulate matter mass in central
555 California, *Journal of the Air & Waste Management Association*, 56(4), 398-410,
556 <https://doi.org/10.1080/10473289.2006.10464515>, 2006.



- 557 Colarco, P. R., Kahn, R. A., Remer, L. A., and Levy, R. C.: Impact of satellite viewing-
558 swath width on global and regional aerosol optical thickness statistics and trends, Atmos.
559 Meas. Tech., 7, 2313-2335, <https://doi.org/10.5194/amt-7-2313-2014>, 2014.
- 560 Di, Q., Wang, Y., Zanobetti, A., Wang, Y., Koutrakis, P., Choirat, C., ... and Schwartz, J. D.: Air
561 pollution and mortality in the Medicare population, New England Journal of
562 Medicine, 376(26), 2513-2522, doi: 10.1056/NEJMoa170274, 2017.
- 563 Engel-Cox, J. A., Holloman, C. H., Coutant, B. W., and Hoff, R. M.: Qualitative and quantitative
564 evaluation of MODIS satellite sensor data for regional and urban scale air quality, Atmos.
565 Environ., 38, 2495–2509, <https://doi.org/10.1016/j.atmosenv.2004.01.039>, 2004.
- 566 Federal Register: National ambient air quality standards for particulate matter. Final Rule
567 Federal Register/vol. 62, no. 138/18 July 1997/Final Rule, 40 CFR Part 50, 1997.
- 568 Glantz, P., Kokhanovsky, A., von Hoyningen-Huene, W., and Johansson, C.: Estimating
569 PM_{2.5} over southern Sweden using space-borne optical measurements, Atmospheric
570 Environment, 43(36), 5838-5846, <https://doi.org/10.1016/j.atmosenv.2009.05.017>, 2009.
- 571 Gong, W., Huang, Y., Zhang, T., Zhu, Z., Ji, Y., and Xiang, H.: Impact and Suggestion of
572 Column-to-Surface Vertical Correction Scheme on the Relationship between Satellite
573 AOD and Ground-Level PM_{2.5} in China, Remote Sensing, 9(10), 1038,
574 <https://doi.org/10.3390/rs9101038>, 2017.
- 575 Greenstone, M.: The impacts of environmental regulations on industrial activity: Evidence from
576 the 1970 and 1977 clean air act amendments and the census of manufactures, Journal of
577 political economy, 110(6), 1175-1219, <https://doi.org/10.1086/342808>, 2002.
- 578 Hand, J. L., and Malm, W. C.: Review of aerosol mass scattering efficiencies from ground-



579 based measurements since 1990, Journal of Geophysical Research:
580 Atmospheres, 112(D16), <https://doi.org/10.1029/2007JD008484>, 2007.

581 Hand, J. L., Schichtel, B. A., Malm, W. C., and Frank, N. H.: Spatial and temporal trends in PM_{2.5}
582 organic and elemental carbon across the United States, Advances in
583 Meteorology, <http://dx.doi.org/10.1155/2013/367674>, 2013.

584 Hänel, G.: The properties of atmospheric aerosol particles as functions of the relative humidity at
585 thermodynamic equilibrium with the surrounding moist air, Advances in geophysics, 19,
586 73-188, [https://doi.org/10.1016/S0065-2687\(08\)60142-9](https://doi.org/10.1016/S0065-2687(08)60142-9), 1976.

587 Hess, M., Koepke, P., and Schult, I.: Optical properties of aerosols and clouds: The software
588 package OPAC, Bulletin of the American meteorological society, 79(5), 831-844,
589 [https://doi.org/10.1175/1520-0477\(1998\)079%3C0831:OPOAAC%3E2.0.CO;2](https://doi.org/10.1175/1520-0477(1998)079%3C0831:OPOAAC%3E2.0.CO;2), 1998.

590 Hoff, Raymond M., and Christopher, Sundar A.: Remote sensing of particulate pollution from
591 space: have we reached the promised land?, Journal of the Air & Waste Management
592 Association, 59.6 (2009): 645-675, <https://doi.org/10.3155/1047-3289.59.6.645>, 2009.

593 Hunt, W. H., Winker, D. M., Vaughan, M. A., Powell, K. A., Lucker, P. L., and Weimer, C.:
594 CALIPSO lidar description and performance assessment, Journal of Atmospheric and
595 Oceanic Technology, 26(7), 1214-1228, <https://doi.org/10.1175/2009JTECHA1223.1>,
596 2009.

597 Illingworth, Anthony J., et al.: The EarthCARE satellite: The next step forward in global
598 measurements of clouds, aerosols, precipitation, and radiation, Bulletin of the American
599 Meteorological Society, 96.8, 1311-1332, <https://doi.org/10.1175/BAMS-D-12-00227.1>,
600 2015.

601 Kaku, K. C., Reid, J. S., Hand, J. L., Edgerton, E. S., Holben, B. N., Zhang, J., and Holz, R. E.:



602 Assessing the challenges of surface-level aerosol mass estimates from remote sensing
603 during the SEAC4RS and SEARCH campaigns: Baseline surface observations and remote
604 sensing in the southeastern United States, *Journal of Geophysical Research: Atmospheres*,
605 123, 7530–7562, <https://doi.org/10.1029/2017JD028074>, 2018.

606 Kittaka, C., Winker, D. M., Vaughan, M. A., Omar, A., & Remer, L. A.: Intercomparison of
607 column aerosol optical depths from CALIPSO and MODIS-Aqua, *Atmospheric
608 Measurement Techniques*, 4(2), 131, <https://doi.org/10.5194/amt-4-131-2011>, 2011.

609 Kumar, N., Chu, A., and Foster, A.: An empirical relationship between PM_{2.5} and aerosol optical
610 depth in Delhi Metropolitan, *Atmos. Environ.*, 41, 4492–4503,
611 <https://doi.org/10.1016/j.atmosenv.2007.01.046>, 2007.

612 Levy, R. C., Mattoo, S., Munchak, L. A., Remer, L. A., Sayer, A. M., Patadia, F., and Hsu, N.C.:
613 The Collection 6 MODIS aerosol products over land and ocean, *Atmos. Meas. Tech.*, 6,
614 2989-3034, <https://doi.org/10.5194/amt-6-2989-2013>, 2013.

615 Li, J., Carlson, B. E., and Laciš, A. A.: How well do satellite AOD observations represent the
616 spatial and temporal variability of PM_{2.5} concentration for the United States?,
617 *Atmospheric environment*, 102, 260-273, <https://doi.org/10.1016/j.atmosenv.2014.12.010>,
618 2015.

619 Liu, Y., Franklin, M., Kahn, R., and Koutrakis, P.: Using aerosol optical thickness to predict
620 ground-level PM_{2.5} concentrations in the St. Louis area: A comparison between MISR and
621 MODIS, *Remote sensing of Environment*, 107(1-2), 33-44,
622 <https://doi.org/10.1016/j.rse.2006.05.022>, 2007.

623

624



- 625 Liu, Y., Park, R. J., Jacob, D. J., Li, Q., Kilaru, V., and Sarnat, J. A.: Mapping annual mean ground-
626 level PM_{2.5} concentrations using Multiangle Imaging Spectroradiometer aerosol optical
627 thickness over the contiguous United States, *Journal of Geophysical Research:*
628 *Atmospheres*, 109 (D22), <https://doi.org/10.1029/2004JD005025>, 2004.
- 629 Liu, Y., Sarnat, J. A., Kilaru, V., Jacob, D. J., and Koutrakis, P.: Estimating ground-level PM_{2.5}
630 in the eastern United States using satellite remote sensing, *Environmental science &*
631 *technology*, 39(9), 3269-3278, doi: 10.1021/es049352m, 2005.
- 632 Liou, Kuo-Nan.: *An introduction to atmospheric radiation*, Vol. 84. Academic press, 2002.
- 633 Lynch P., and coauthors: An 11-year global gridded aerosol optical thickness reanalysis (v1.0) for
634 atmospheric and climate sciences, *Geosci. Model Dev.*, 9, 1489-1522, doi:10.5194/gmd-9-
635 1489-2016, 2016.
- 636 Malm, W.C. and Hand, J.L.: An examination of the physical and optical properties of aerosols
637 collected in the IMPROVE program, *Atmospheric Environment*, 41(16), pp.3407-3427,
638 <https://doi.org/10.1016/j.atmosenv.2006.12.012>, 2007.
- 639 Omar, A. H., Winker, D. M., Tackett, J. L., Giles, D. M., Kar, J., Liu, Z., Vaughan, M. A., Powell,
640 K. A., and Trepte, C. R.: CALIOP and AERONET aerosol optical depth comparisons: One
641 size fits none, *J. Geophys. Res. Atmos.*, 118, 4748–4766, doi:10.1002/jgrd.50330, 2013.
- 642 Reid, J. S., Eck, T. F., Christopher, S. A., Koppmann, R., Dubovik, O., Eleuterio, D. P., Holben,
643 B. N., Reid, E. A., and Zhang, J.: A review of biomass burning emissions part III: intensive
644 optical properties of biomass burning particles, *Atmos. Chem. Phys.*, 5, 827-849,
645 <https://doi.org/10.5194/acp-5-827-2005>, 2005.
- 646 Reid, J. S. et al.: Skill of Operational Aerosol Forecast Models in Predicting Aerosol Events and



- 647 Trends of the Eastern United States, A11B-001, AGU Fall meeting, San Francisco, 12-16
648 Dec, 2016.
- 649 Reid, J. S., Kuehn, R. E., Holz, R. E., Eloranta, E. W., Kaku, K. C., Kuang, S., ... and Atwood,
650 S.A.: Ground-based High Spectral Resolution Lidar observation of aerosol vertical
651 distribution in the summertime Southeast United States, *Journal of Geophysical Research:*
652 *Atmospheres*, 122(5), 2970-3004, <https://doi.org/10.1002/2016JD025798>, 2017.
- 653 Sessions, W. R., Reid, J. S., Benedetti, A., Colarco, P. R., da Silva, A., Lu, S., Sekiyama, T.,
654 Tanaka, T. Y., Baldasano, J. M., Basart, S., Brooks, M. E., Eck, T. F., Iredell, M., Hansen,
655 J. A., Jorba, O. C., Juang, H.-M. H., Lynch, P., Morcrette, J.-J., Moorthi, S., Mulcahy, J.,
656 Pradhan, Y., Razinger, M., Sampson, C. B., Wang, J., and Westphal, D. L.: Development
657 towards a global operational aerosol consensus: basic climatological characteristics of the
658 International Cooperative for Aerosol Prediction Multi-Model Ensemble (ICAP-MME),
659 *Atmos. Chem. Phys.*, 15, 335-362, <https://doi.org/10.5194/acp-15-335-2015>, 2015.
- 660 Silva, R. A., West, J. J., Zhang, Y., Anenberg, S. C., Lamarque, J. F., Shindell, D. T., Collins,
661 W.J., Dalsoren, S., Faluvegi, G., Folberth, G. & Horowitz, L. W.: Global premature
662 mortality due to anthropogenic outdoor air pollution and the contribution of past climate
663 change, *Environmental Research Letters*, 8(3), 034005, doi:10.1088/1748-
664 9326/8/3/034005, 2013.
- 665 Toth, T. D., Campbell, J. R., Reid, J. S., Tackett, J. L., Vaughan, M. A., Zhang, J., and Marquis,
666 J. W.: Minimum aerosol layer detection sensitivities and their subsequent impacts on
667 aerosol optical thickness retrievals in CALIPSO level 2 data products, *Atmos. Meas. Tech.*,
668 11, 499-514, <https://doi.org/10.5194/amt-11-499-2018>, 2018.
- 669 Toth, T. D., Zhang, J., Campbell, J. R., Hyer, E. J., Reid, J. S., Shi, Y., and Westphal, D. L.: Impact



670 of data quality and surface-to-column representativeness on the PM_{2.5} / satellite AOD
671 relationship for the contiguous United States, *Atmos. Chem. Phys.*, 14, 6049-6062,
672 <https://doi.org/10.5194/acp-14-6049-2014>, 2014.

673 Toth, T. D., Zhang, J., Campbell, J. R., Reid, J. S., Shi, Y., Johnson, R. S., Smirnov, A., Vaughan,
674 M.A. and Winker, D. M.: Investigating enhanced Aqua MODIS aerosol optical depth
675 retrievals over the mid-to-high latitude Southern Oceans through intercomparison with co-
676 located CALIOP, MAN, and AERONET data sets, *Journal of Geophysical Research:*
677 *Atmospheres*, 118(10), 4700-4714, <https://doi.org/10.1002/jgrd.50311>, 2013.

678 Toth, T. D., Zhang, J., Campbell, J. R., Reid, J. S., and Vaughan, M. A.: Temporal variability of
679 aerosol optical thickness vertical distribution observed from CALIOP, *Journal of*
680 *Geophysical Research: Atmospheres*, 121(15), 9117-9139,
681 <https://doi.org/10.1002/2015JD024668>, 2016.

682 Val Martin, M., Heald, C. L., Ford, B., Prenni, A. J., and Wiedinmyer, C.: A decadal satellite
683 analysis of the origins and impacts of smoke in Colorado, *Atmos. Chem. Phys.*, 13, 7429-
684 7439, <https://doi.org/10.5194/acp-13-7429-2013>, 2013.

685 Van Donkelaar, A., Martin, R.V., Brauer, M., Kahn, R., Levy, R., Verduzco, C., and Villeneuve,
686 P. J.: Global Estimates of Ambient Fine Particulate Matter Concentrations from Satellite
687 Based Aerosol Optical Depth: Development and Application, *Environ. Health Perspect.*,
688 118(6): 847–855, <https://dx.doi.org/10.1289%2Fehp.0901623>, 2010.

689 Van Donkelaar, A., Martin, R. V., Spurr, R. J., and Burnett, R. T.: High-resolution satellite-derived
690 PM_{2.5} from optimal estimation and geographically weighted regression over North
691 America, *Environmental science & technology*, 49.17 (2015): 10482-10491,
692 doi: 10.1021/acs.est.5b02076, 2015.



- 693 Waggoner, A. P., and Weiss, R. E.: Comparison of fine particle mass concentration and light
694 scattering extinction in ambient aerosol, *Atmospheric Environment* (1967), 14(5), 623-
695 626, [https://doi.org/10.1016/0004-6981\(80\)90098-0](https://doi.org/10.1016/0004-6981(80)90098-0), 1980.
- 696 Wang, J., and Christopher, S. A.: Intercomparison between satellite-derived aerosol optical
697 thickness and PM_{2.5} mass: implications for air quality studies, *Geophysical research*
698 *letters*, 30(21), <https://doi.org/10.1029/2003GL018174>, 2003.
- 699 Winker, D. M., Hunt, W. H., and McGill, M. J.: Initial performance assessment of CALIOP,
700 *Geophysical Research Letters*, 34(19), <https://doi.org/10.1029/2007GL030135>, 2007.
- 701 Winker, D. M., Pelon, J., Coakley Jr, J. A., Ackerman, S. A., Charlson, R. J., Colarco, P. R., ...
702 and Kubar, T. L.: The CALIPSO mission: A global 3D view of aerosols and clouds,
703 *Bulletin of the American Meteorological Society*, 91(9), 1211-1230,
704 <https://doi.org/10.1175/2010BAMS3009.1>, 2010.
- 705 Winker, D. M., Vaughan, M. A., Omar, A., Hu, Y., Powell, K. A., Liu, Z., Hunt, W. H., and Young,
706 S. A.: Overview of the CALIPSO Mission and CALIOP Data Processing Algorithms, *J.*
707 *Atmos. Oceanic Technol.*, 26, 2310–2323, <https://doi.org/10.1175/2009JTECHA1281.1>,
708 2009.
- 709 Young, S. A., Vaughan, M. A., Kuehn, R. E., and Winker, D. M.: The retrieval of profiles of
710 particulate extinction from Cloud–Aerosol Lidar and Infrared Pathfinder Satellite
711 Observations (CALIPSO) data: Uncertainty and error sensitivity analyses, *Journal of*
712 *Atmospheric and Oceanic Technology*, 30(3), 395-428,
713 <https://doi.org/10.1175/2009JTECHA1281.1>, 2013.
- 714 Zhang, J., Campbell, J.R., Hyer, E. J., Reid, J.S., Westphal, D. L., and Johnson, R. S.: Evaluating



715 the impact of multisensor data assimilation on a global aerosol particle transport model, J.

716 Geophys. Res. Atmos., 119, 4674–4689, doi:10.1002/2013JD020975, 2014.

717 Zhang, J. and Reid, J.S.: An analysis of clear sky and contextual biases using an operational over

718 ocean MODIS aerosol product, Geophysical Research Letters, 36, L15824,

719 doi:10.1029/2009GL038723, 2009.

720

721

722

723

724

725

726

727

728

729

730

731

732

733

734

735

736

737

738

739

740

741

742

743

744

745

746

747

748

749

750

751

752

753



754 **Figure and Table Captions**

755

756 Figure 1. For 2008-2009, scatterplot of mean PM_{2.5} concentration from ground-based U.S. EPA
757 stations and mean column AOD (550 nm) from collocated Collection 6 (C6) Aqua MODIS
758 observations.

759

760 Figure 2. For 2008-2009 over the CONUS, (a) mean PM_{2.5} concentration ($\mu\text{g m}^{-3}$) for those U.S.
761 EPA stations with reported daily measurements, and (c) $1^\circ \times 1^\circ$ average CALIOP-derived PM_{2.5}
762 concentrations for the 100–1000 m AGL atmospheric layer, using Equation 3, for combined
763 daytime and nighttime conditions. Also shown are the pairwise PM_{2.5} concentrations from (b)
764 EPA daily measurements and (d) those derived from CALIOP (day and night combined), both
765 averaged for each EPA station for the 2008-2009 period. For all four plots, values greater than 20
766 $\mu\text{g m}^{-3}$ are colored red.

767

768 Figure 3. For 2008-2009 over the CONUS, $1^\circ \times 1^\circ$ average CALIOP extinction, relative to the
769 number of cloud-free 5 km CALIOP profiles in each $1^\circ \times 1^\circ$ bin, for the 100 – 1000 m AGL
770 atmospheric layer, for (a) daytime and (b) nighttime measurements. Also shown are the
771 corresponding CALIOP-derived PM_{2.5} concentrations, using Equation 3 for (c) daytime and (d)
772 nighttime conditions. Values greater than 0.2 km^{-1} and $20 \mu\text{g m}^{-3}$ for (a, b) and (c, d), respectively,
773 are colored red. Scatterplots of mean PM_{2.5} concentration from ground-based U.S. EPA stations
774 and those derived from collocated near-surface CALIOP observations are shown in the bottom
775 row, using (e) daytime and (f) nighttime CALIOP data.



776 Figure 4. Scatterplot of mean $PM_{2.5}$ concentration from ground-based U.S. EPA stations and those
777 derived from collocated near-surface CALIOP observations using combined daytime and
778 nighttime CALIOP data.

779

780 Figure 5. Root-mean-square errors of CALIOP-derived $PM_{2.5}$ against EPA $PM_{2.5}$ as a function of
781 CALIOP-derived $PM_{2.5}$ (filled circles), and corresponding number of data samples per bin (X
782 symbols), using both daytime (in red) and nighttime (in blue) CALIOP observations.

783

784 Figure 6. Two-year (2008-2009) histograms of mean $PM_{2.5}$ concentrations from the U.S. EPA (in
785 black) and those derived from aerosol extinction using nighttime (in blue) and daytime (in red)
786 CALIOP data. The U.S. EPA data shown are not collocated, while those derived using CALIOP
787 are spatially (but not temporally) collocated, with EPA station observations.

788

789 Figure 7. Two-year (2008-2009) histograms of mean $PM_{2.5}$ concentrations from the U.S. EPA and
790 those derived from spatially and temporally collocated aerosol extinction using (a) daytime and
791 (b) nighttime CALIOP data.

792

793 Figure 8. For 2008-2009, scatterplots of mean $PM_{2.5}$ concentration from ground-based U.S. EPA
794 stations and mean column AOD from collocated CALIOP observations, using (a) daytime and (b)
795 nighttime CALIOP data.

796



797 Figure 9. For 2008-2009, scatterplots of mean $PM_{2.5}$ concentration from ground-based U.S. EPA
798 stations and those derived from collocated all-sky (including cloud-free and cloudy profiles) near-
799 surface CALIOP observations, using (a) daytime and (b) nighttime CALIOP data.

800

801 Figure 10. For 2008-2009 over the CONUS, scatterplot of distance (km) between any two U.S.
802 EPA stations and the corresponding spatial correlation of $PM_{2.5}$ concentration between each pair
803 of stations. The black curve represents the exponential fit to the data for the entire CONUS, and
804 the red and blue dashed lines represent 10 km bin averages for the Western and Eastern CONUS,
805 respectively.

806

807 Table 1. The parameters, and corresponding values, used to quality assure the CALIOP aerosol
808 extinction profile.

809

810 Table 2. Statistical summary of a sensitivity analysis varying the height of the surface layer,
811 including R^2 , slope, mean bias (CALIOP - EPA) of $PM_{2.5}$ in $\mu g m^{-3}$, and percent error change in
812 derived $PM_{2.5}$, defined as: $((\text{mean new } PM_{2.5} - \text{mean original } PM_{2.5}) / \text{mean original } PM_{2.5}) * 100$.

813 The row in bold represents the results shown in the remainder of the paper.

814

815 Table 3. Statistical summary of a sensitivity analysis varying the $PM_{2.5}$ to PM_{10} ratio used,
816 including slope, mean bias (CALIOP - EPA) of $PM_{2.5}$ in $\mu g m^{-3}$, and percent error change in
817 derived $PM_{2.5}$, defined as: $((\text{mean new } PM_{2.5} - \text{mean original } PM_{2.5}) / \text{mean original } PM_{2.5}) * 100$.

818 The row in bold represents the results shown in the remainder of the paper.

819



820 Table 4. Statistical summary of a sensitivity analysis varying the aerosol type assumed in the
821 derivation of $PM_{2.5}$, including R^2 , slope, mean bias (CALIOP - EPA) of $PM_{2.5}$ in $\mu g m^{-3}$, and
822 percent error change in derived $PM_{2.5}$, defined as: $((\text{mean new } PM_{2.5} - \text{mean original } PM_{2.5}) / \text{mean}$
823 $\text{original } PM_{2.5}) * 100$. The row in bold represents the results shown in the remainder of the paper.

824

825

826

827

828

829

830

831

832

833

834

835

836

837

838

839

840

841

842

843



844 **Figures**

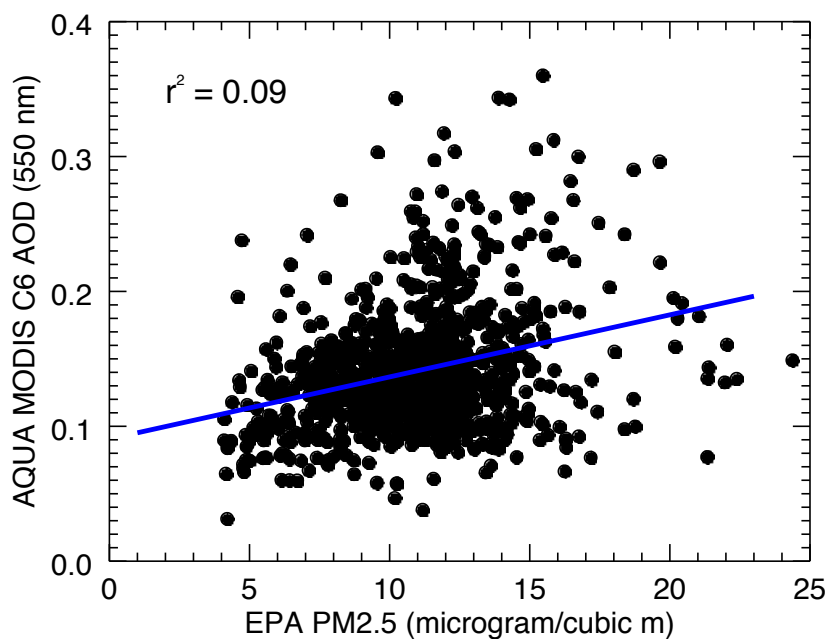


Figure 1. For 2008-2009, scatterplot of mean PM_{2.5} concentration from ground-based U.S. EPA stations and mean column AOD (550 nm) from collocated Collection 6 (C6) Aqua MODIS observations.

845

846



847

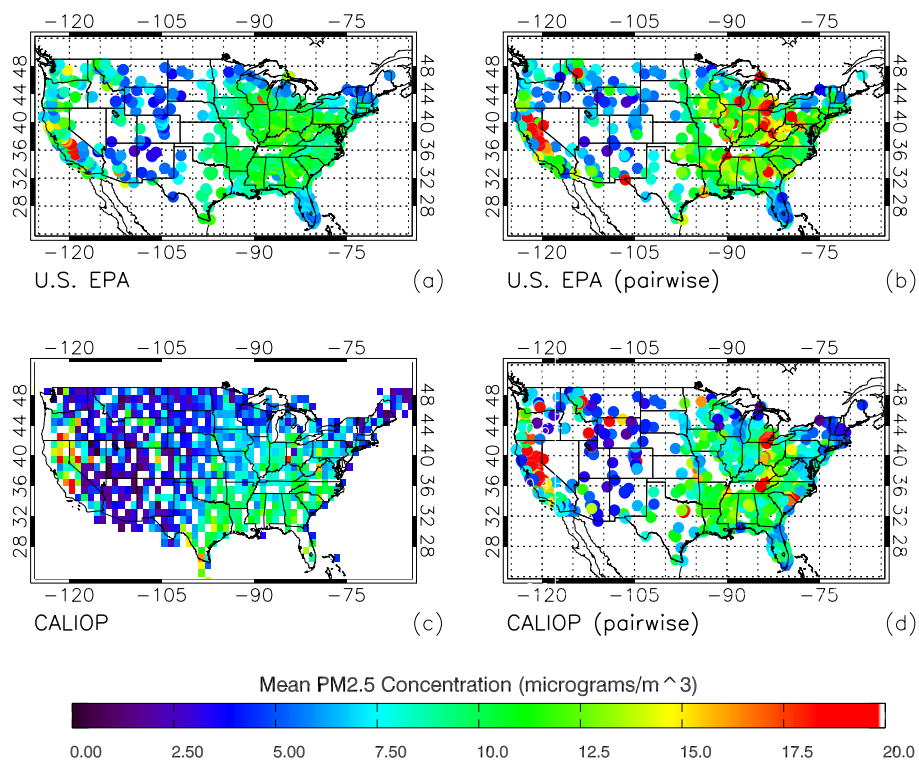


Figure 2. For 2008-2009 over the CONUS, (a) mean PM_{2.5} concentration ($\mu\text{g m}^{-3}$) for those U.S. EPA stations with reported daily measurements, and (c) $1^\circ \times 1^\circ$ average CALIOP-derived PM_{2.5} concentrations for the 100–1000 m AGL atmospheric layer, using Equation 3, for combined daytime and nighttime conditions. Also shown are the pairwise PM_{2.5} concentrations from (b) EPA daily measurements and (d) those derived from CALIOP (day and night combined), both averaged for each EPA station for the 2008-2009 period. For all four plots, values greater than $20 \mu\text{g m}^{-3}$ are colored red.

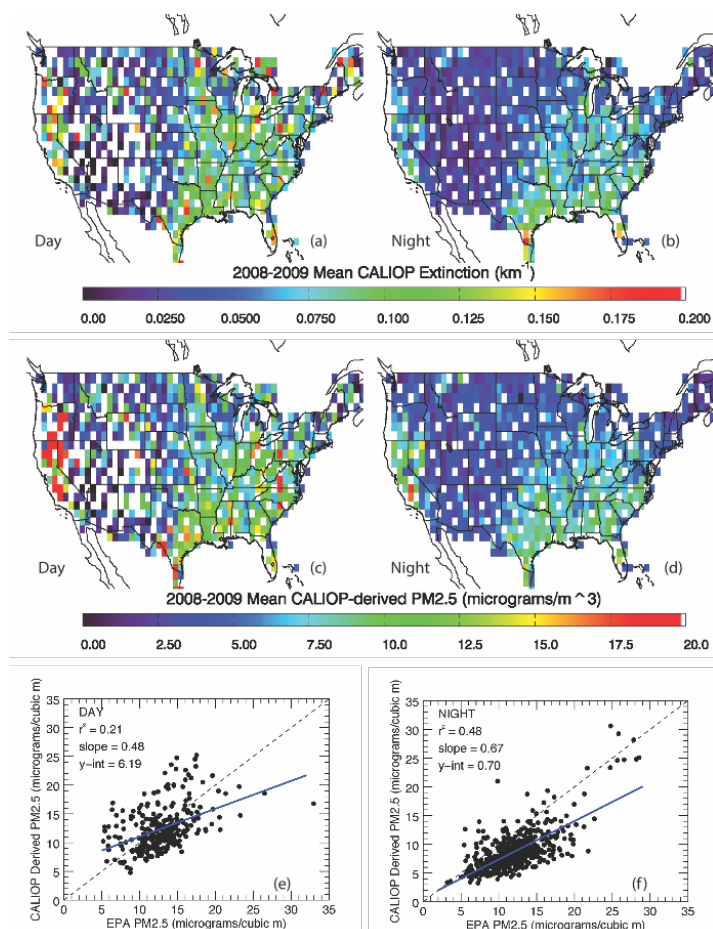


Figure 3. For 2008-2009 over the CONUS, $1^\circ \times 1^\circ$ average CALIOP extinction, relative to the number of cloud-free L2_05kmAPro profiles in each $1^\circ \times 1^\circ$ bin, for the 100 – 1000 m AGL atmospheric layer, for (a) daytime and (b) nighttime measurements. Also shown are the corresponding CALIOP-derived PM_{2.5} concentrations, using Equation 3 for (c) daytime and (d) nighttime conditions. Values greater than 0.2 km^{-1} and $20 \mu\text{g m}^{-3}$ for (a, b) and (c, d), respectively, are colored red. Scatterplots of mean PM_{2.5} concentration from ground-based U.S. EPA stations and those derived from collocated near-surface CALIOP observations are shown in the bottom row, using (e) daytime and (f) nighttime CALIOP data.

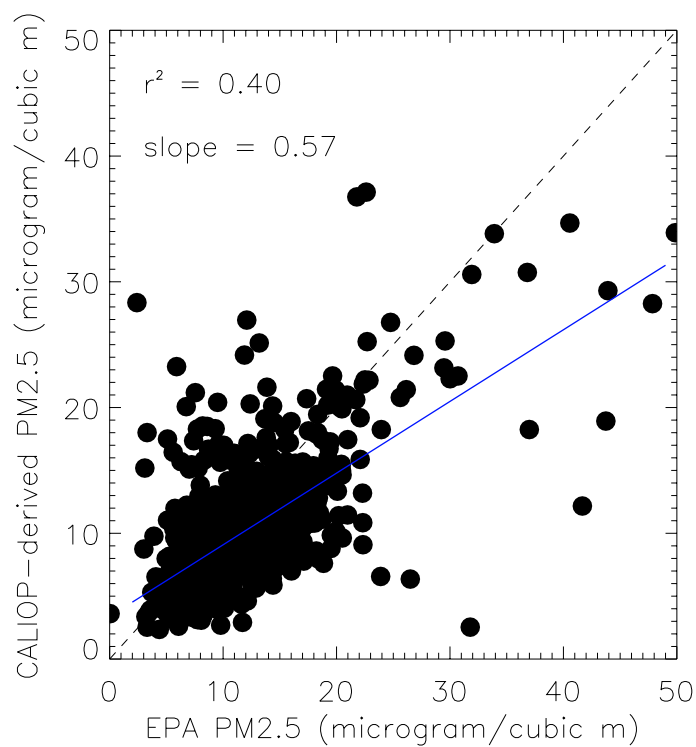


Figure 4. Scatterplot of mean PM_{2.5} concentration from ground-based U.S. EPA stations and those derived from collocated near-surface CALIOP observations using combined daytime and nighttime CALIOP data.

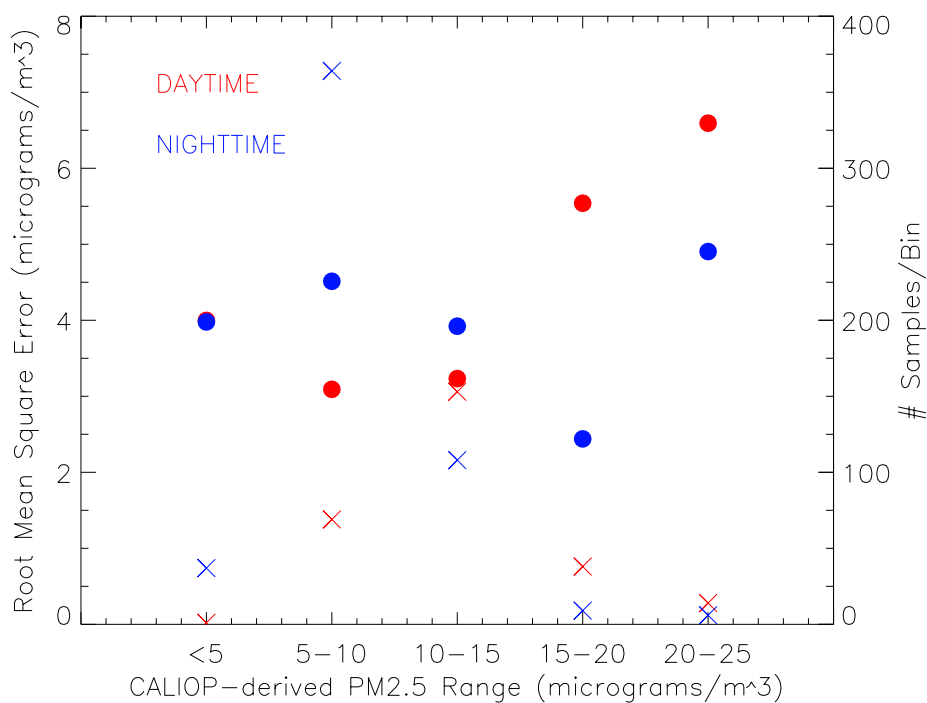


Figure 5. Root-mean-square errors of CALIOP-derived PM_{2.5} against EPA PM_{2.5} as a function of CALIOP-derived PM_{2.5} (filled circles), and corresponding number of data samples per bin (X symbols), using both daytime (in red) and nighttime (in blue) CALIOP observations.

850
851
852
853
854
855
856
857
858
859

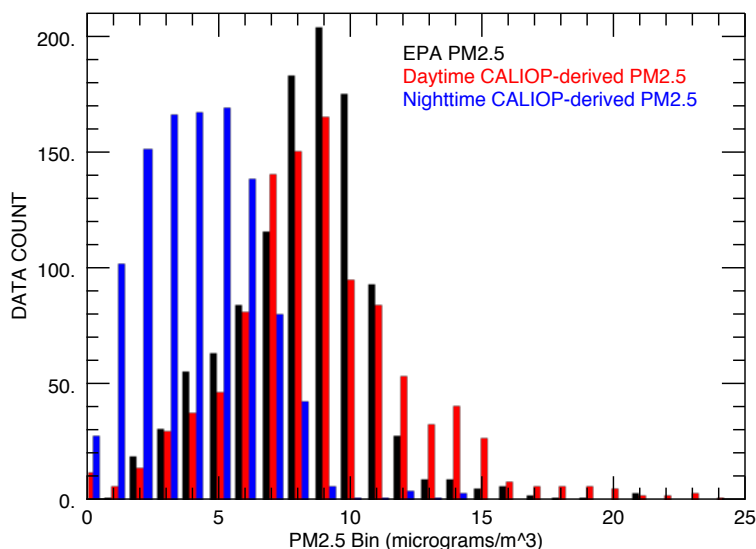


Figure 6. Two-year (2008-2009) histograms of mean PM_{2.5} concentrations from the U.S. EPA (in black) and those derived from aerosol extinction using nighttime (in blue) and daytime (in red) CALIOP data. The U.S. EPA data shown are not collocated, while those derived using CALIOP are spatially (but not temporally) collocated, with EPA station observations.

860
861
862
863
864
865
866

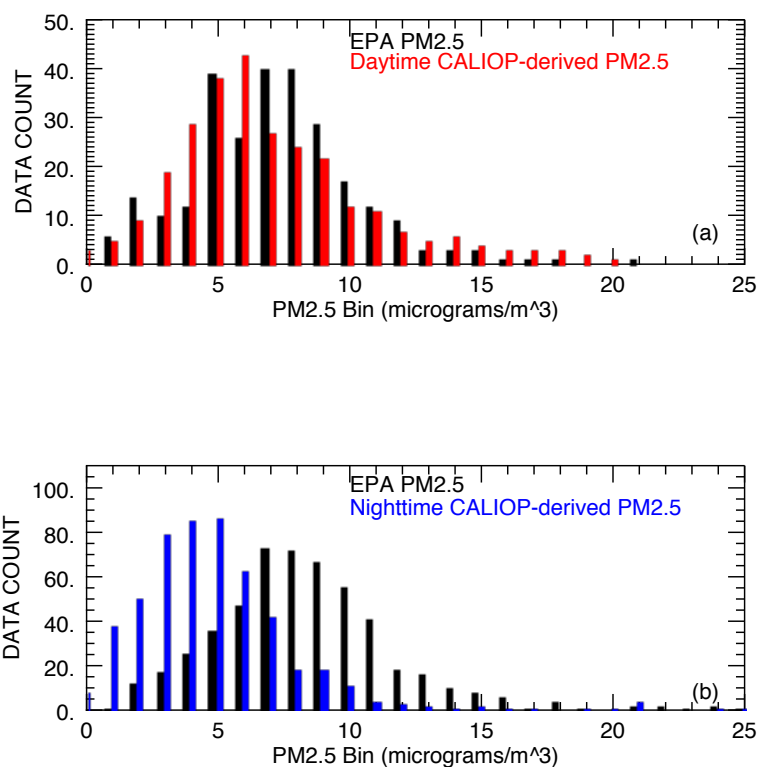


Figure 7. Two-year (2008-2009) histograms of mean PM_{2.5} concentrations from the U.S. EPA and those derived from spatially and temporally collocated aerosol extinction using (a) daytime and (b) nighttime CALIOP data.

867
868
869
870
871
872
873
874
875
876

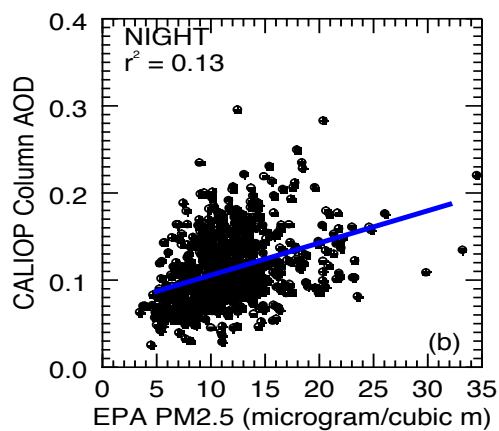
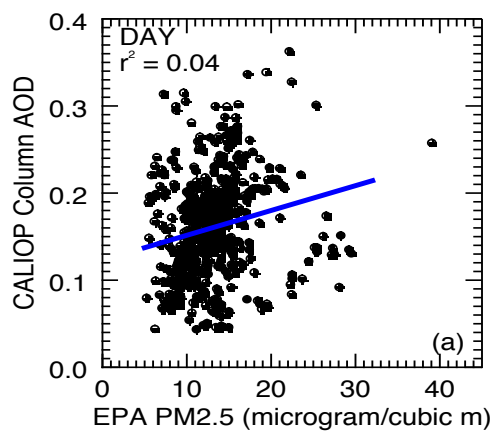


Figure 8. For 2008-2009, scatterplots of mean PM_{2.5} concentration from ground-based U.S. EPA stations and mean column AOD from collocated CALIOP observations, using (a) daytime and (b) nighttime CALIOP data.

877

878

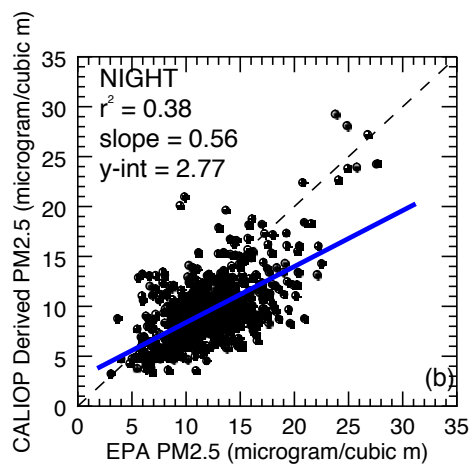
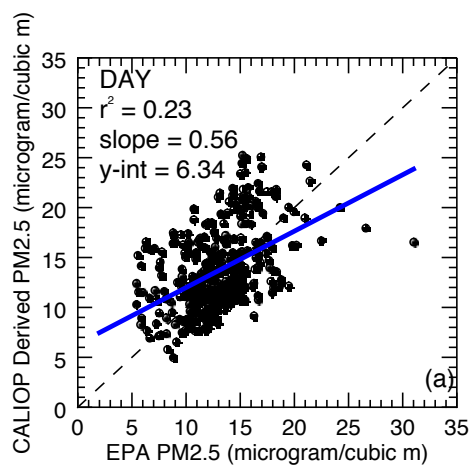


Figure 9. For 2008-2009, scatterplots of mean PM_{2.5} concentration from ground-based U.S. EPA stations and those derived from collocated all-sky (including cloud-free and cloudy profiles) near-surface CALIOP observations, using (a) daytime and (b) nighttime CALIOP data.

879
880
881
882

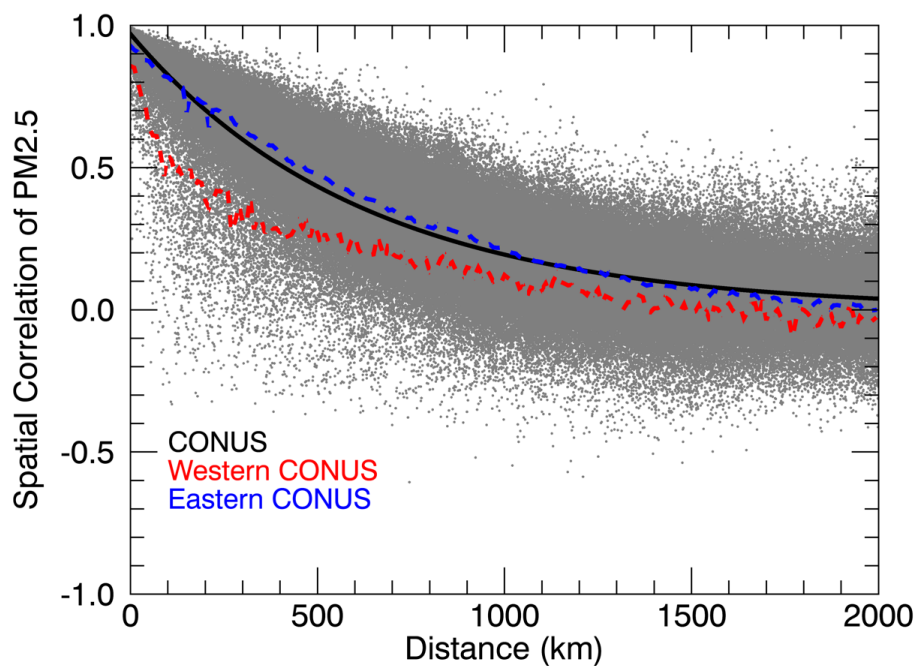


Figure 10. For 2008-2009 over the CONUS, scatterplot of distance (km) between any two U.S. EPA stations and the corresponding spatial correlation of PM_{2.5} concentration between each pair of stations. The black curve represents the exponential fit to the data for the entire CONUS, and the red and blue dashed lines represent 10 km bin averages for the Western and Eastern CONUS, respectively.

883
884
885
886



887

888 **Tables**

889

890

891

Parameter	Values
Integrated_Attenuated_Backscatter_532	$\leq 0.01 \text{ sr}^{-1}$
Extinction_Coefficient_532	≥ 0 and $\leq 1.25 \text{ km}^{-1}$
Extinction_QC_532	= 0, 1, 2, 16, or 18
CAD_Score	≥ -100 and ≤ -20
Extinction_Coefficient_Uncertainty_532	$\leq 10 \text{ km}^{-1}$
Atmospheric_Volume_Description (Bits 1-3)	= 3
Atmospheric_Volume_Description (Bits 10-12)	$\neq 0$

Table 1. The parameters, and corresponding values, used to quality assure the CALIOP aerosol extinction profile.

892

893

894

895

896

897

898

899

900

901



902
903
904
905

Surface Layer (m)	Analysis (Day/Night)			
	R ²	Slope	Mean Bias (CALIOP - EPA; µg m ⁻³)	Error Change (%)
0-100	0.27/0.41	0.69/0.38	-2.67/-9.06	-13.71/-61.94
0-200	0.33/0.53	0.77/0.75	-0.52/-5.68	3.79/-23.58
0-300	0.35/0.54	0.78/0.82	-0.09/-4.70	7.24/-12.15
0-400	0.38/0.57	0.80/0.85	-0.13/-4.25	6.92/-6.46
0-500	0.35/0.52	0.75/0.76	-0.21/-4.04	5.70/-4.39
0-600	0.40/0.53	0.76/0.75	-0.46/-3.91	3.72/-2.15
0-700	0.44/0.46	0.80/0.66	-0.41/-3.89	2.73/-2.88
0-800	0.35/0.50	0.62/0.66	-0.59/-3.76	-0.77/-2.04
0-900	0.17/0.49	0.43/0.63	-0.74/-3.74	-3.91/-2.25
0-1000	0.13/0.48	0.35/0.62	-1.08/-3.74	-7.48/-2.57
100-500	0.34/0.44	0.72/0.66	0.54/-3.40	14.21/-0.84
100-1000	0.21/0.48	0.48/0.67	-0.39/-3.34	

Table 2. Statistical summary of a sensitivity analysis varying the height of the surface layer, including R², slope, mean bias (CALIOP - EPA) of PM_{2.5} in µg m⁻³, and percent error change in derived PM_{2.5}, defined as: ((mean new PM_{2.5} – mean original PM_{2.5})/mean original PM_{2.5})*100. The row in bold represents the results shown in the remainder of the paper.

906
907
908
909
910
911
912
913
914
915
916



917
918
919
920
921
922
923
924
925
926

PM _{2.5} /PM ₁₀ Ratio	Slope	Analysis (Day/Night)	
		Mean Bias (CALIOP - EPA; µg m ⁻³)	% Error Change
Low ratio (-1 STDEV) = 0.24	0.19/0.27	-7.81/-8.61	-60.00%/-60.00%
High ratio (+1 STDEV) = 0.88	0.71/0.98	5.39/0.77	46.67%/46.67%
0.6	0.48/0.67	-0.39/-3.34	

Table 3. Statistical summary of a sensitivity analysis varying the PM_{2.5} to PM₁₀ ratio used, including slope, mean bias (CALIOP - EPA) of PM_{2.5} in µg m⁻³, and percent error change in derived PM_{2.5}, defined as: ((mean new PM_{2.5} – mean original PM_{2.5})/mean original PM_{2.5})*100. The row in bold represents the results shown in the remainder of the paper.

927
928
929
930
931



932
 933
 934
 935
 936
 937
 938
 939
 940

Analysis (Day/Night)							
Aerosol Type			R ²	Slope	Mean Bias (CALIOP-EPA; $\mu\text{g m}^{-3}$)	% Error Change	
	a_{scat}	a_{abs}	Γ				
Smoke	5.26	0.26	0.18	0.10/0.44	0.27/0.52	-1.81/-4.26	-11.53/-10.54
Sea salt	1.42	0.01	0.46	0.18/0.48	1.22/1.82	22.42/12.93	184.12/184.99
Dust	0.52	0.08	0	0.05/0.39	2.06/5.12	102.04/70.82	826.94/843.33
Sulfate	3.4	0.37	0.63	0.21/0.48	0.48/0.67	-0.39/-3.34	

Table 4. Statistical summary of a sensitivity analysis varying the aerosol type assumed in the derivation of $\text{PM}_{2.5}$, including R^2 , slope, mean bias (CALIOP - EPA) of $\text{PM}_{2.5}$ in $\mu\text{g m}^{-3}$, and percent error change in derived $\text{PM}_{2.5}$, defined as: $((\text{mean new PM}_{2.5} - \text{mean original PM}_{2.5}) / \text{mean original PM}_{2.5}) * 100$. The row in bold represents the results shown in the remainder of the paper.

941
 942
 943
 944
 945
 946